# Direct in situ and real-time visualization of salt-dependent thiolated-DNA immobilization and biosensing on gold in nanofluidic channels

Deng-Kai Yang, Liang-Kun Yu, Chia-Tzu Kuo, Jui-Hong Weng, Thierry Leïchlé, Nathan Swami, Lin-Chi Chen, Pei-Kuen Wei, Chia-Fu Chou

Sensors & Actuators: B. Chemical xxx (xxxx) 134303

Contents lists available at ScienceDirect

Sensors & Actuators: B. Chemical

journal homepage: www.elsevier.com/locate/snb

# Direct *in situ* and real-time visualization of salt-dependent thiolated-DNA immobilization and biosensing on gold in nanofluidic channels

Deng-Kai Yang [a], Liang-Kun Yu [a], Chia-Tzu Kuo [a], Jui-Hong Weng [a], Thierry Leïchlé [b], Nathan S. Swami [c], Lin-Chi Chen [d], Pei-Kuen Wei [e], Chia-Fu Chou [a, e, *]

[a] Institute of Physics, Academia Sinica, 128 Academia Rd. Section 2, Nangang District, Taipei 11529, Taiwan
[b] LAAS-CNRS & Université de Toulouse, Toulouse 31031, France
[c] Department of Electrical & Computer Engineering, University of Virginia, Charlottesville, VA 22904, USA
[d] Department of Biomechatronics Engineering, National Taiwan University, No. 1, Section 4, Roosevelt Rd., Taipei 10617, Taiwan
[e] Research Center of Applied Sciences, Academia Sinica, 128 Academia Rd. Section 2, Nangang District, Taipei 11529, Taiwan

ARTICLE INFO

*Keywords:*
Nanofluidics
Thiolated-DNA–gold conjugation
*in situ* visualization
Depletion zone/effect
Biosensing

ABSTRACT

Thiol-gold (Au) conjugation is perhaps the most routinely applied surface chemistry approach to immobilize receptors within Au-based molecular sensing platforms. However, no previous studies have investigated *in situ* immobilization in a nanofluidic systems. In this work, flowthrough receptor immobilization is demonstrated, using a nanoslit induced depletion zone to enable direct real-time visualization for characterizing the effect of sodium chloride (NaCl) concentrations during immobilization of thiolated single-stranded DNA on Au. The results show that the amount of fixed-DNA on Au, as well as the non-specific adsorption of DNA on fused silica surface, strongly depend on NaCl levels. Furthermore, the non-specific interaction at high NaCl levels reduces the DNA available for immobilization on Au, but enriches the DNA molecules in the channel under wash by deionized water. By adding Tween-20 to decrease the non-specific adsorption and increasing the driving pressure to increase the DNA flux under high-salt level, the immobilization time can be further decreased to 10 min or less, which is at least an order of magnitude faster than recently proposed bioconjugation methods for thiolated-DNA–Au conjugation. Moreover, this work demonstrates the capability of the platform for DNA- and aptamer-based sensing assays, thereby opening up new strategies for developing biosensors using nanofluidic platforms.

## 1. Introduction

Receptors immobilized on gold (Au) substrates are widely used within optical [1,2] and electrochemical sensors [3,4]. In Au-based sensing platforms, the attachment of single-stranded DNA (ssDNA) to Au is a generic step for biorecognition at electrode [5,6] and Au nanoparticle (AuNP) interfaces [7–9]. The Au-thiol interaction is frequently used to immobilize thiolated-DNA onto Au, which provides a robust way to fabricate self-assembled monolayers (SAMs) as functional molecules for further conjugations [10–13]. Since DNA is a negatively charged molecule, electrostatic repulsion from pre-adsorbed DNA molecules increases the difficulty of adsorption and immobilization events. Therefore, the DNA density on the Au surface is limited, and incubation over several hours is typically required to achieve a steady-state level of DNA immobilization [14,15]. Various assembly strategies to increase the efficiency of immobilizing thiolated-DNA onto the Au surface have been considered in recent years. For instance, positively charged ions in salt or acidic solutions are used to reduce electrostatic repulsion between DNA molecules or between DNA and a negatively charged solid support substrate, such as AuNPs [16,17]. By doing so, the DNA density on a plain Au surface can be increased and the reaction time for achieving steady-state immobilization levels can be reduced to ~1 hour [14,15].

Microfluidic chips are widely used in biosensing [18,19] and biomedical [20] applications. The fluidic systems can effectively monitor the binding interaction on Au in real-time and manipulate the flux of target molecules by regulating the flow velocity, which are significant advantages when compared with conventional open-top systems. In re-

*Abbreviations:* Au, Gold; AuNPs, Gold nanoparticles; DI, Deionized; EMCCD, Electron-multiplying charge-coupled device; ICP, Inductively coupled plasma; NaCl, Sodium chloride; PSQ, Polysilsesquioxane; SAM, Self-assembled monolayers; SPR, Surface plasmon resonance; ssDNA, Single-stranded DNA; TCEP, Tris(2-carboxyethyl)phosphine

* Corresponding author at: Institute of Physics, Academia Sinica, 128 Academia Rd. Section 2, Nangang District, Taipei 11529, Taiwan.
*E-mail address:* cfchou@phys.sinica.edu.tw (C.-F. Chou).

https://doi.org/10.1016/j.snb.2023.134303
Received 26 December 2022; Received in revised form 14 July 2023; Accepted 15 July 2023
0925-4005/

cent years, with the rapid development of nanofabrication technology [21–23], nanofluidic platforms have increasingly been used to investigate the transport properties in nanofluidic channels [24–27], the behavior of molecular transport [28–32], and many possible applications of biomolecular analysis [23,33–38]. It has been reported that nanoslit designs enable near-instant equilibration of concentration profiles in the transverse direction at high axial flow rates. As a result, the reaction time is dramatically reduced and a depletion effect is exhibited, which is caused by ~100 % reaction at the device surface between targets and probes with high affinity [33,39–41]. Moreover, the resulting target/analyte depletion effect in the nanochannel enables virtually background-free fluorescence imaging at high detection sensitivity for real-time visualization of their immobilization or binding events at the surface [33], which is not possible by conventional surface plasmon resonance (SPR) characterization [14].

Hence, this fluidic phenomenon unique to nanochannels can be utilized for kinetic studies in real-time visualization [42], which would be difficult to conduct within a microfluidic chip, and enable spatial resolution down to a single oligonucleotide base-pair [43]. Surprisingly, no prior work has utilized this depletion effect to systematically study the influence of salt level on *in situ* Au-thiol conjugation and DNA transport to the immobilization surface, which is vital for oligonucleotide-related gene detection assays, aptamer-based sensors, and other sensor schemes in nanochannel systems.

To investigate this issue, a nanochannel patterned with Au patches was used to study the immobilization of thiolated ssDNA prepared in different concentrations of sodium chloride (NaCl). As shown in Fig. 1, DNA sample was loaded into the 500 nm-height channels using a pressure pump. After each DNA sample loading step, deionized (DI) water was introduced to remove the unbound DNA molecules. Previous studies have shown that the fluorophore signals can be quenched by Au when excited fluorophores are in proximity of the Au surface [44–47]. Thus, Cy5-labeled ssDNA with hairpin structure was used in this work to observe the salt effect on DNA immobilization and conformational change [48].

## 2. Experimental section

Materials, DNA sequences, equipment, and software are detailed in Supplementary material.

### 2.1. Fabrication of a nanochannel patterned with Au patches

The fabrication procedure of fused silica chips bearing 500 nm deep channels has been described previously [49]. Fused silica substrate was spin-coated with photoresist, UV exposed and developed, then etched by inductively coupled plasma (ICP) to 500 nm deep channels with 1 mm in width and 1 cm in length. A 4 × 3 array of square Au patches was designed on the bottom of the channel (Fig. S1). Moreover, a polysilsesquioxane (PSQ)-coated cover glass was used to seal the nanochannels [49,50]. See Supplementary material for more details.

### 2.2. DNA adsorption and immobilization on an Au surface in a nanofluidic channel

One micromolar thiolated-DNA was prepared in different concentrations of NaCl with 40 μM tris(2-carboxyethyl)phosphine (TCEP). Initially, the nanofluidic chip was rinsed by DI water, and then the DNA samples were loaded into the channel for 40 minutes. To observe the immobilization efficiency of the DNA samples, DI water was loaded into the channel for 10 minutes after every DNA loading step. All fluid flows were driven by applying moderate negative pressures, and the linear relationship between pumping pressure and volume flow rate is shown in Fig. S2. The DNA sensor chips were imaged using an inverted microscope with an electron-multiplying charge-coupled device (EMCCD) camera. Fluorescent images were obtained with a 10× objective (N.A. = 0.25) using a typical Cy5 filter set.

## 3. Results and discussions

### 3.1. Characterization of the reaction of thiolated-DNA on Au surface in a nanoconfined channel

To characterize the immobilization of DNA on an Au surface in a nanochannel platform, two dimensionless numbers were used to express relationships of diffusion to reaction rate (Damköhler numbers: $D_a = [k_{on} \times P_0 \times h]/[D]$) and convection rate (Péclet number: $P_e = [U_m \times h]/[D]$) [33], where $k_{on}$ is the association rate constant for thiolated-DNA adsorption to Au (~$1 \times 10^3$ $M^{-1}s^{-1}$) [51], $P_0$ the quasi-maximum surface density of thiolated-DNA immobilized on Au (~$1 \times 10^{13}$ molecules/cm²) [52], $U_m$ the mean flow velocity (280 μm/s), $D$ thediffusion coefficient of DNA in aqueous solution (~$10^{-11}$ m²/s)

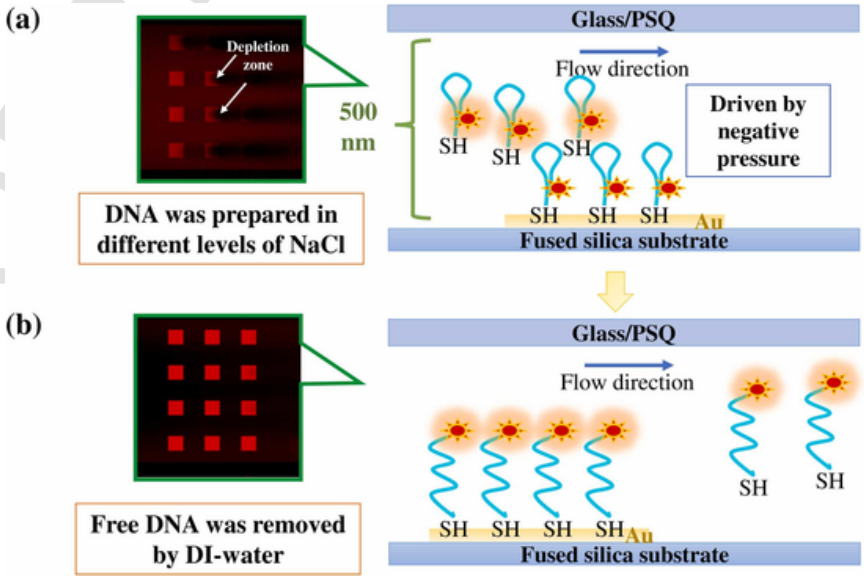


**Fig. 1.** Experimental layout of salt-dependent thiolated-DNA–Au interaction study in a nanofluidic channel device. (a) DNA was immobilized with depletion effect on Au patches in nanochannels. (b) The excess DNA was removed based on a DI water wash step.

[53], and $h$ the channel height (500 nm). In our case, $D_a$ is ~ 0.008, which is much smaller than one, indicating that the reaction in the nanoplatform is reaction-limited. Additionally, $P_e$ is ~ 14, which is much larger than one, denoting that molecular diffusion has a negligible effect on concentration variation. Moreover, the relationship between the time for molecules to travel along and diffuse across the nanochannel (reduce time: $t = [D \times l]/[U_m \times h^2]$) was also estimated as the distance ($l$) of thiolated-DNA to pass through an Au patch was 100 μm. Here, $t$ is ~ 14.3, which is much larger than 2, indicating almost 100 % of thiolated-DNA is attached to the Au surface when passing through the Au patch [54], resulting in the observed depletion zone in the nanochannel platform [33]. These results suggest that the nanochannel design reduces the vertical diffusion effect and thus achieves higher reaction efficiency compared with the open-top system. In addition, the fluorescent background of the bulk solution is significantly reduced due to the nanoscale channel height. Therefore, compared with the microchannel design, the nanoconfinement design enables *in situ* visualization of DNA immobilized on the Au surface, which facilitates direct observation of the reactions near the sensor surface.

### 3.2. Imaging the interaction of thiolated-DNA with Au in DI water

Upon loading 1 μM Cy5-C14-SH aptamer (see Supplementary material) [48] dissolved in DI water into the nanochannel by flow, no analyte depletion region was apparent (Fig. S3a), implying a low level of interaction between the thiolated-DNA and the Au surface [33]. It is noteworthy that the increasing fluorescence signal on top of the Au patches is due to the reflectivity of the Au thin film at the excited wavelength [33]. After the washing step, the signal at the Au patches dropped to the level before the sample loading (Fig. S3b), indicating the limited number of thiol-Au bond forming sites for DNA in DI water, as the electrostatic repulsion from pre-adsorbed DNA increases the difficulty of immobilizing subsequent DNA sequences from the bulk solution [14].

### 3.3. Imaging the interaction of thiolated-DNA with Au at different NaCl concentrations

As shown in Fig. 2a, no analyte depletion was discerned under the 4 mM NaCl condition, and no significant fluorescent signal was detected on Au patches after washing step. Analogous results of DNA immobilization obtained in NaCl concentrations of 12 mM and 37 mM are shown in Fig. 2b and Fig. S4, respectively. Fig. 2b shows a small degree of depletion, indicating there are some interactions between the thiolated-DNA and the Au surface, such as physical adsorption between nucleotides and Au [6], and the formation of Au–sulfur bonds. However, a significant signal was not detected on Au patches after removing unbound sequences (Fig. 2e). Under the 37 mM salt condition, the depletion zones were more pronounced (Fig. S4a), but the weak fluorescent signals, detected on Au patches after the washing step, indicated only low level of interaction between the thiolated-DNA and the Au surface (Fig. S4b). This indicates that these limited NaCl levels do not significantly reduce the electrostatic repulsion upon DNA immobilization.

Considering the DNA immobilization in 110 mM (Fig. S5) and 330 mM (Fig. 2c) NaCl solutions, the depletion zones were clearly seen when DNA molecules flow over the Au patches. As in Fig. S5, an apparent fluorescent signal continued to be detected on Au patches after washing with DI water. The intensity was $2,771 \pm 367$ (a.u.), which is seven times higher than the signal ($414 \pm 45$ a.u.) from the open-top experiment with 40 minutes incubation time under the same salt condition (Fig. S6). This indicates that the nanoslit design can dramatically increases the DNA immobilization efficiency under flow conditions *versus* that obtained by incubation under open-top reaction.

To be noted, in Fig. 2e, the maximum signal on Au patches was around 1000 (a.u.) in the DNA loading step under 330 mM NaCl condition, but increased up to 5000 (a.u.) after washing with DI water. We attribute this observation to the following. The thiolated-DNA was predicted to form a stem-loop (Fig. S7) in salt solution [48,55], thereby shortening the distance between Cy5 fluorophores and the Au surface. It has been reported that when excited fluorophores are in proximity of the Au surface, the overall quantum yield becomes approximately equal to the quantum yield of the plasmons, thereby lowering the fluores-

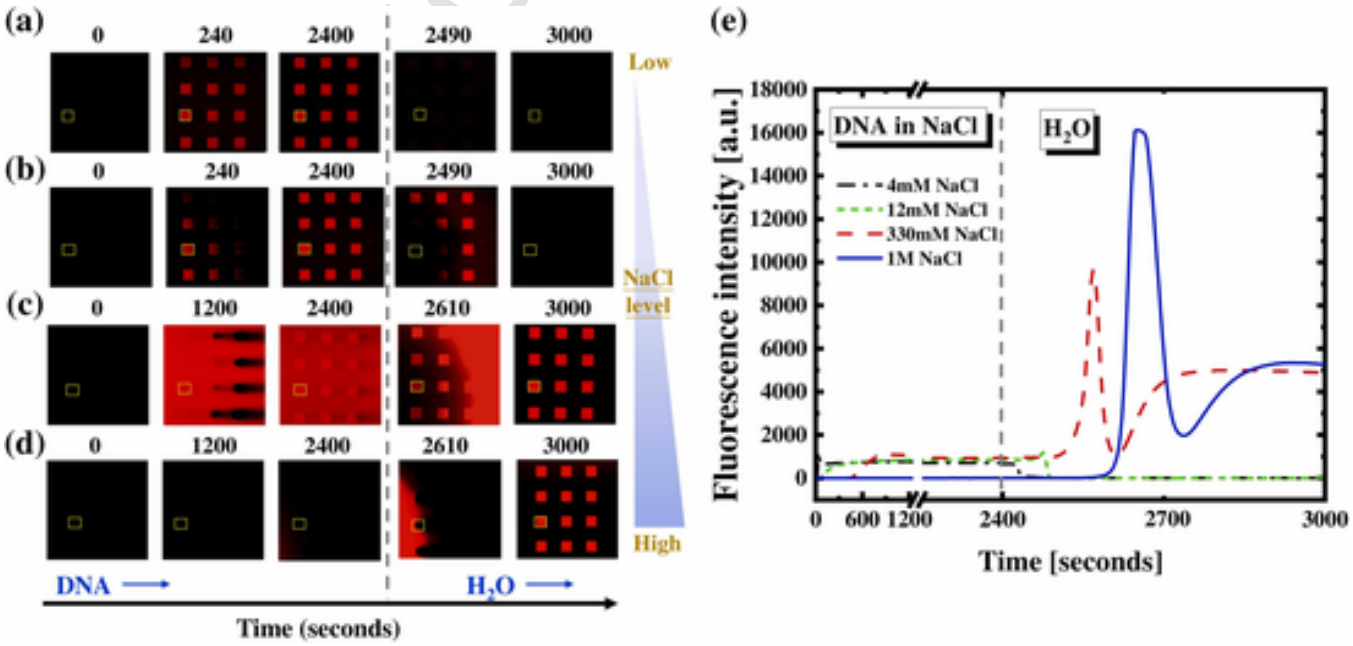


**Fig. 2.** Imaging of the depletion pattern in the nanochannel immobilized with Cy5-C14-SH on Au at different NaCl concentrations. Time-lapse fluorescence images captured from the nanofluidic channel device: 1 μM Cy5-C14-SH/40 μM TCEP/(a) 4 mM (black dot-dashed line), (b) 12 mM (green short dashed line), (c) 330 mM (red dashed line) and (d) 1 M (blue solid line) NaCl solutions flowed through for 40 minutes, and washed by DI water. (e) Temporal fluorescence intensities (pixel-averaged) generated from the regions of interest (yellow squares) in (a-d). The driven pressure is −50 mbar. (See Movies S1 to S8).

cence signal [44]. Hence, the signal of the Cy5 fluorophore was likely quenched by the Au thin film, and the fluorescence signal observed on the Au patches at DNA loading steps was caused by the emission and reflection signals of the free Cy5-labeled DNA in the bulk (Fig. 2e) [33]. However, the strong electrostatic repulsion between the DNA bases caused the stem-loop structure to be pulled open during the following DI water wash step, thereby enlarging the distance between Cy5 fluorophores and the Au surface, resulting in an increase in fluorescence signal. Thus, the DNA conformational changes at different salt levels were visualized. Furthermore, the regenerated fluorescence signal could represent the relative amount of fixed-DNA on the Au surface (DI water loading steps of Fig. 2e). Likewise, by analyzing the signals of the fixed-DNA, it indicates that DNA density on the Au surface may be increased by enhancing the thiol-Au interaction through increasing the salt concentration, so that the immobilization occurs within the reaction time frame (*i.e.*, 40 minutes) (Fig. S8).

Interestingly, in 1 M NaCl solution, DNA did not reach the sensing area even after 40 minutes of flowing the DNA sample (Fig. 2d). However, after flowing DI water through the channel, an enriched-DNA band passed over the Au patches, and the fluorescence signal of fixed-DNA on the Au patches read around 5,000 (a.u.) (Fig. 2e). This surprising observation is elucidated in the following section.

### 3.4. Higher NaCl concentration leads to higher non-specific adsorption effect

In literature, siloxane on the surface of hydroxylated amorphous fused silica has been reported to exhibit hydrophobic characteristics [56], and DNA can adsorb on the surface of amorphous fused silica by hydrophobic interaction and hydrogen-bonding interactions, which are formed between the DNA phosphate and surface silanol group of the silica [57]. These reports indicate that DNA can adsorb on the fused silica surface in the nanofluidic channel, and the salt concentrations neutralize the charge on DNA backbones and the fused silica surface, thereby enriching the amount of DNA that adsorbs and self-aggregates on the silica surface. To verify the role of this phenomenon on our results, a DNA sample prepared in 110 mM NaCl solution was loaded into the channel, and then 330 mM NaCl solution without DNA was used to wash the channel, followed by another DI water wash, which regenerated the signal of the fixed-DNA molecules on Au patches. As in Fig. 3 and Fig. S9, we can find fluorescence intensity from the non-specific adsorption of DNA on the $SiO_2$ surface in 330 mM NaCl solution is higher than that in DI water. This indicates that a higher NaCl concentration leads to a higher non-specific adsorption of DNA on $SiO_2$ surface. Consequently, a highly enriched-DNA band was observed when DI water was loaded to wash the channel, even after previous washing by 330 mM NaCl solution. It suggests that the salt-free washing solution reduces the non-specific adsorption of DNA on the silica surface and the enrichment of DNA in the nanochannel. Furthermore, this result can explain the greater time required for DNA transport through the nanochannel under high salt conditions, by enhancing DNA adsorption and self-aggregation on the fused silica surface, such as at 1 M NaCl (Fig. 2d), even after 40 minutes of loading.

### 3.5. The effect of surfactant and flow velocity on DNA immobilization in nanochannel

Tween-20, a nonionic surfactant with hydrophobic tails that bind to a hydrophobic domain of fused silica, was used to decrease the non-specific adsorption of DNA. By adding 0.05 % Tween-20 in the DNA sample prepared in 1 M NaCl solution reduces non-specific adsorption, as in Fig. S10. Thus, more DNA molecules become available for immobilization on Au compared to the sample prepared without Tween-20, as shown in the DNA loading step of Fig. 2d.

Furthermore, compared to the conventional open-top system, the nanochannel system provides the ability to modulate molecular flux to the surface. Thus, we increased flow velocity by increasing the negative driving pressure from 50 (condition with no surfactant) to 700 mbar and immobilized DNA under 1 M and 2 M NaCl/0.05 % Tween-20 conditions for 10 minutes (Fig. 4a-b and Fig. S11). The averaged immobilization signals from twelve Au patches were increased up to $6,735 \pm 273$ (a.u.) and $6,924 \pm 290$ (a.u.) under 1 M and 2 M NaCl/0.05 % Tween-20 condition, respectively, and plotted in comparison with the immobilization process without added Tween-20 (Fig. 4c). Furthermore, under the aforementioned conditions, the fixed-DNA on the Au surface almost reached a steady-state level, and the DNA (60-mer) density was $\sim 0.42 \times 10^{12}$ molecules/cm$^2$ on the Au patch (Supplementary material Section 1.6), which is comparable to the order of magnitude reported in previous works ($10^{12} - 10^{13}$ molecules/cm$^2$ for 25-mer DNA)[52,58].



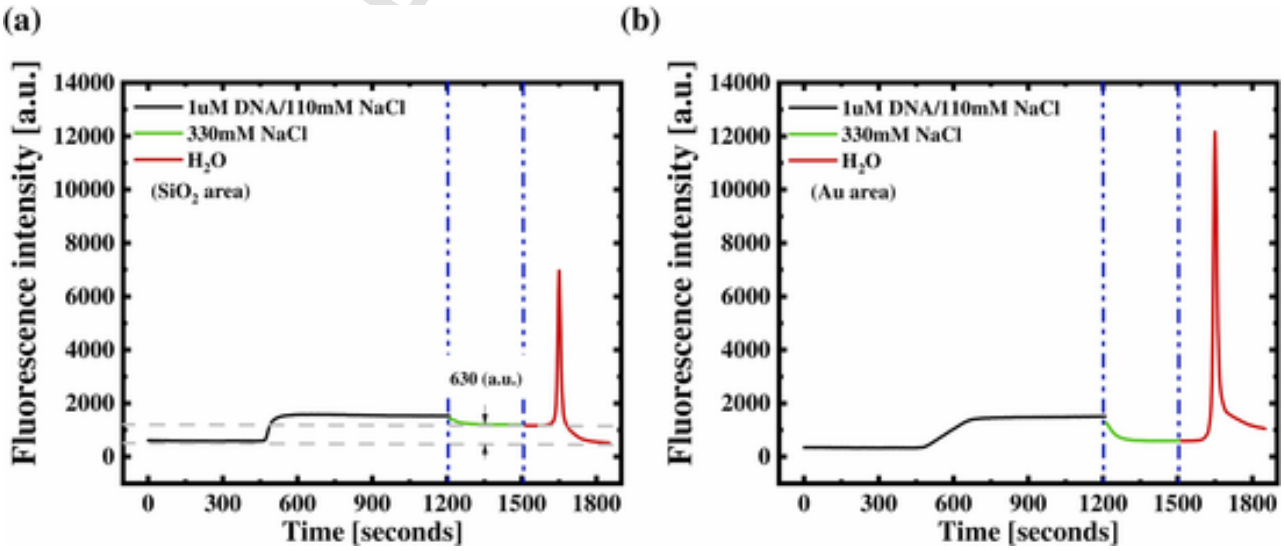


**Fig. 3.** The effect of NaCl concentration on non-specific adsorption of DNA between fused-silica and Au surfaces: 1 μM Cy5-C14-SH /40 μM TCEP/110 mM NaCl solution flowed through for 20 minutes, washed by 330 mM NaCl, and rinsed by DI-water. (a) Temporal fluorescence intensities (pixel-averaged) generated from the regions of interest (green squares, fused-silica area) in Fig. S9. (b) Temporal fluorescence intensities (pixel-averaged) generated from the regions of interest (yellow squares, Au area) in Fig. S9. The driven pressure is − 50 mbar.

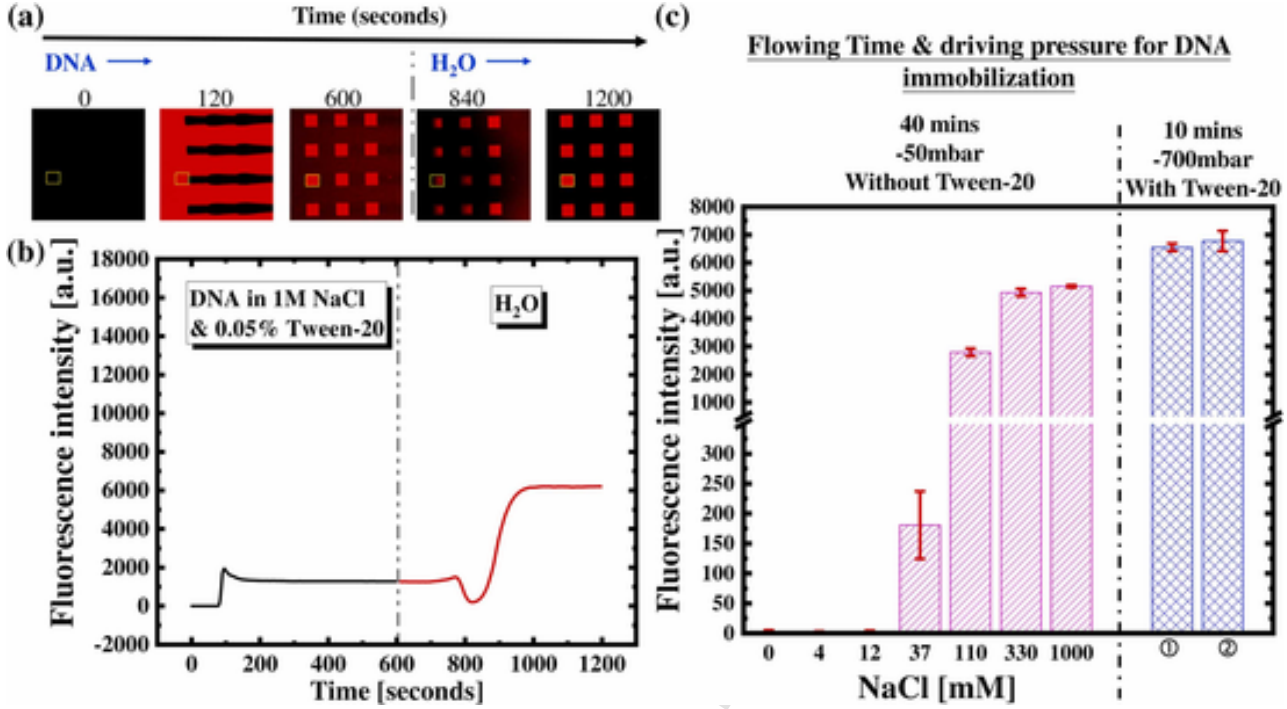


**Fig. 4.** (a) Immobilization of Cy5-C14-SH in the nanochannel with 1 M NaCl/0.05 % Tween-20. Time-lapse fluorescence images captured from the nanofluidic channel device: 1 μM Cy5-C14-SH /40 μM TCEP/1 M NaCl/0.05 % Tween-20 solution for 10 minutes (driven pressure −700 mbar) and washed by DI water (driven pressure −50 mbar). (b) Temporal fluorescence intensities (pixel-averaged) generated from the regions of interest (yellow squares) in (a) (see Movies S9 and S10). (c) The immobilization signals of DNA in the nanochannel under different NaCl concentrations. The values represent the average fluorescence signal of the fixed-Cy5-C14-SH on the twelve Au patches in the nanochannel after the DI water washing step, with the error bars indicating the standard deviation from the mean of the fluorescence signal. Specifically, ① and ② refer to 1 μM Cy5-C14-SH/40 μM TCEP/0.05 % Tween-20 prepared in 1 M NaCl and 2 M NaCl, respectively.

This result indicates that DNA immobilization time can be reduced from several hours required within conventional open-top system to just a few minutes in the nanochannel under (1) high driving pressure to increase the flux of DNA molecules, (2) high salt conditions to reduce the electrostatic repulsion effect, and (3) the addition of 0.05 % Tween-20 to lessen the hydrophobic effect between DNA molecules and the surface of the fused silica.

### 3.6. DNA- and aptamer-based biosensing in the nanochannel

To extend the knowledge learned from the salt-dependent DNA immobilization study above for biosensing applications, we used DNA-based (lung) cancer gene and aptamer-based protein (human alpha thrombin) sensing, as practically and clinically interested targets, for such demonstrations.

For the DNA gene sensing assay, we used a probe DNA fragment corresponding to a lung cancer gene marker [59] (SH-25T_CYFRA21–1 (P), see Supplementary material). To demonstrate the specific detection capability of the platform at different probe densities, we used a Cy5-labeled target DNA fragment (Cy5- CYFRA21–1 (T), see Supplementary material) and Cy3-labeled non-target DNA fragment (Cy3–40T (N), see Supplementary material) as samples. To ensure consistent reaction conditions, we co-loaded the samples into the nanochannel to react with probes, which were fixed on Au under different NaCl levels, to demonstrate the capability of differential sensing. The experiment procedure is described in detail in the Supplementary material.

The results presented in Fig. 4c demonstrate that the probe density on the Au surface is dependent on the NaCl levels in the immobilization solution. In Fig. 5a, we found that the depletion phenomenon was apparent during target DNA detection, while Fig. 5b shows that the sensing intensity of the target DNA increases with an increase in probe density on Au region. Additionally, Fig. 5a demonstrates that the depletion zone is not apparent within non-target samples, and the fluorescence intensity of non-target samples does not depend on probe density (Fig. 5c, Au region). It is worth noting that the increased fluorescence intensities observed during non-target sensing are due to the reflectivity of the Au thin film at the excited wavelength (Fig. 5c), and the intensities from the Au surface are twice that from the $SiO_2$ surface [33]. Moreover, it is well known that the fluorescence intensity of different dye-labeled targets is influenced by factors such as the quantum yield of the dye molecule and the dye-to-target ratio. Therefore, in order to compare the fluorescence intensities observed from samples with different dye labels, it is necessary to eliminate the effects of these factors *via* the normalization process discussed below.

To truly reveal the nature and information of our data, we compared the intensities between the ones from the probe-fixed Au surface and non-probe-fixed $SiO_2$ surface (background) for both target and non-target sensing analysis by dividing the intensities from the Au surface by 2 to counter the reflectivity issue from the Au surface. The resulting values were further normalized by the intensities from the $SiO_2$ surface (background). In the case of target DNA sensing (Fig. 5d), the normalized signal/background ratios increase over time and are much greater than 1, indicating that target DNA was successfully captured by the probe with high specificity. Conversely, in non-target DNA sensing, the ratios (Fig. 5e) hover around 1, suggesting minimal non-specific adsorption which supports the conclusion that the intensity changes in Fig. 5c primarily arise from the emission and reflection intensities of the free Cy3-labeled non-target DNA in the bulk solution thus serving as the background intensity.

For the protein sensing assay, we adopted aptamer-based sensing scheme by fixing the anti-thrombin aptamer [60] (SH-25T_TBA, see Supplementary material) on Au patches in the nanochannel. Then, we co-loaded Cy5-labeled thrombin and Alexa 488-labeled streptavidin (non-target control) into the nanochannel to react with the fixed-aptamer. The experiment procedure is detailed in the Supplementary material.

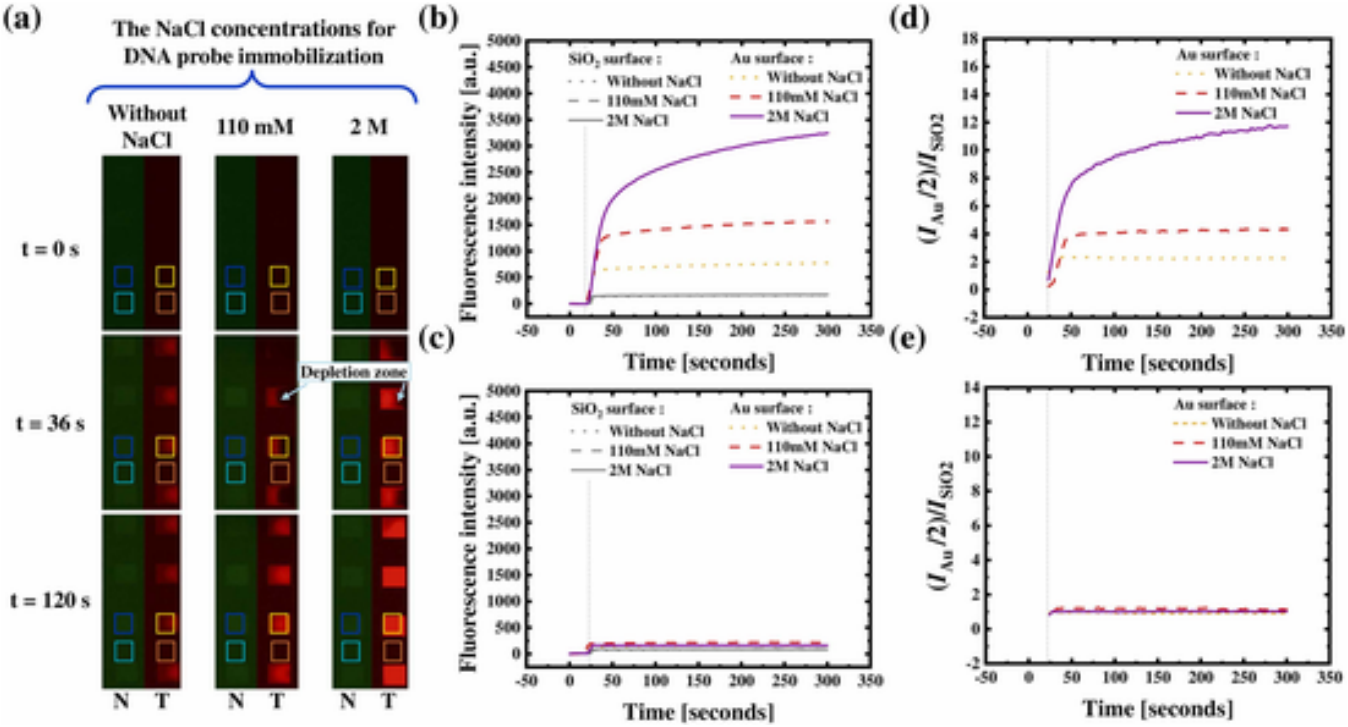


**Fig. 5.** The lung cancer gene detection assays with different probe densities generated under various salt conditions. Time-lapse fluorescence images captured from the first column of Au patches in the nanofluidic channel device: (a) detection of mixed DNA sample contains Cy5-CYFRA21–1 (T) and Cy3–40T fragments (N) (N: Non-target; T: Target; See Movie S11). (b) Temporal fluorescence intensities (pixel-averaged) generated from the regions of interest of target detection on Au (yellow squares) and $SiO_2$ (orange squares) in (a). (c) Temporal fluorescence intensities (pixel-averaged) generated from the regions of interest of non-target detection on Au (blue squares) and $SiO_2$ (light blue squares) in (a). (d) The intensity ratio curves obtained from (b) by normalizing the sensing intensities on Au surface ($I_{Au}$) with those of $SiO_2$ surface ($I_{SiO2}$). (e) The intensity ratio curves obtained from (c) by normalizing the sensing intensities on Au with those of $SiO_2$.

The results presented in Fig. 6a and b clearly distinguish between the sensing of the target thrombin and the non-target streptavidin reaction. The target thrombin sensing exhibits a characteristic depletion phenomenon and the Langmuir-like kinetics curve, whereas the non-target streptavidin reaction does not exhibit a depletion phenomenon and shows a step-like kinetics curve. Additionally, the intensity ratio curves for the target protein reached ~ 4 in Fig. 6c, whereas those for the non-target protein remained around 1 after loading the mixed sample. This suggests that, the increase in fluorescence intensity observed in the non-target streptavidin loading is due to the overall background increase caused by the bulk solution on Au surface. Moreover, this confirms that the aptamer-based sensing can accurately and specifically identify the thrombin target protein by using this platform.

## 4. Conclusions

Owing to the formation of the characteristic depletion zone under flow of fluorescent sample in a nanoconfined channel, the *in-situ* immobilization of DNA on the Au surface can be visualized in real time. Our results show DNA immobilization time can be dramatically reduced from several hours to minutes within a nanochannel under high-salt environment compared to conventional open-top systems. In addition, the amount of the non-specific adsorbed DNA molecules is increased with the concentration of NaCl, and the DNA molecules can be released and enriched by switching the loading solution to DI water into the nanochannel. These results suggest that shrinking the channel height to the nanoscale enhances the collision frequency of DNA molecules to the sensing surface, thereby accelerating the immobilization procedure. Consequently, the adverse circumstance of the non-specific adsorption of DNA molecules to channel surface could also be enhanced with particularly high salt concentrations, a problem that may be alleviated by using Tween-20 and increasing the DNA flux *via* increased driving pressure, by which the immobilization time of DNA may be expedited further down to less than 10 minutes. We further demonstrated the generality of using the nanofluidic platform and the associated immobilization protocols for *in situ* molecular conformational change observation and wash-free, real-time DNA gene and aptamer-based protein sensing. This study provides a new perspective to accelerate immobilization of thiolated DNA on Au and point out the issues to be addressed in operating a nanofluidic platform for applications such as biosensing and aptamer screening. The outcomes of this study hold potential for the future development of nanoconfinement platforms employing alternative quantitative detection techniques such as surface plasmon resonance and electrochemical detection.

## CRediT authorship contribution statement

**Deng-Kai Yang:** Conceptualization, Methodology, Data Acquisition and Analysis, Writing - Original Draft. **Liang-Kun Yu:** Device Fabrication, Writing - Original Draft (Chip Fabrication part). **Chia-Tzu Kuo:** Device Fabrication. **Jui-Hong Weng:** Protein sample preparation, labeling, and characterization. **Thierry Leïchlé :** Methodology, Writing - Review & Editing. **Nathan S. Swami:** Writing - Review & Editing, Funding acquisition. **Lin-Chi Chen:** Writing - Review & Editing, Resources, Protein characterization. **Pei-Kuen Wei:** Project administration, Funding acquisition. **Chia-Fu Chou:** Methodology, Writing - Review & Editing, Resources, Funding acquisition, Supervision.

## Declaration of Competing Interest

The authors declare that they have no known competing financial interests or personal relationships that could have appeared to influence the work reported in this paper.

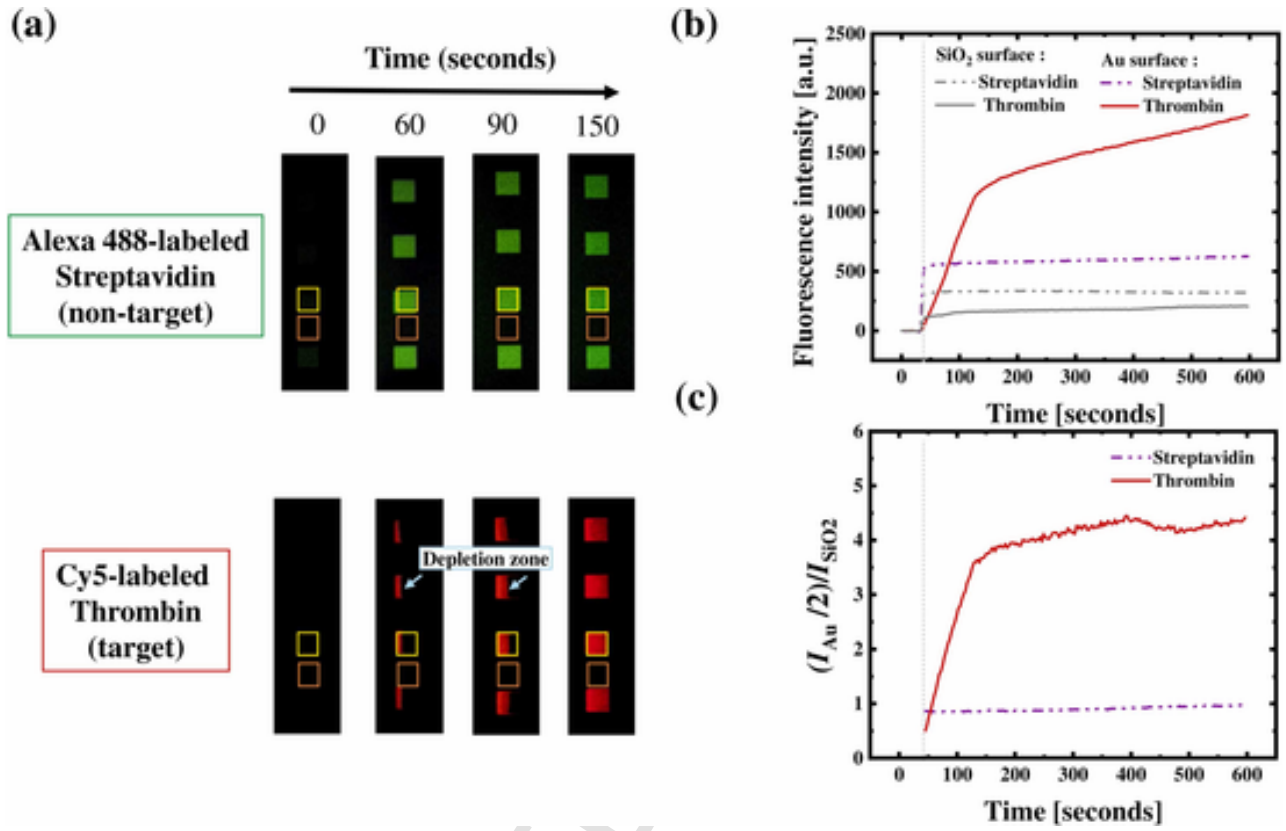


**Fig. 6.** The thrombin detection assay using an anti-thrombin aptamer. Time-lapse fluorescence images captured from the first column of Au patches in the nanofluidic channel device: (a) detection of mixed protein sample contains Alexa 488-labeled streptavidin and Cy5-labeled human alpha thrombin (See Movie S12). (b) Temporal fluorescence intensities (pixel-averaged) generated from the regions of interest on Au (yellow squares) and $SiO_2$ (orange squares) in (a). (c) The intensity ratio curves obtained from (b) by normalizing the sensing intensities on Au surface ($I_{Au}$) with those of $SiO_2$ surface ($I_{SiO2}$).

## Data availability

Data will be made available on request.

## Acknowledgements

This work was sponsored by Academia Sinica Investigator Award, Taiwan (grant # AS-IA-109-M04 to C.F.C.), National Science and Technology Council, Taiwan (NSTC, grants# 107-2923-M-001-011-MY3, 109-2124-M-001-003, 110-2124-M-001-003, and 111-2112-M-001-029-MY3 to C.F.C.) , Air Force Office of Scientific Research (AFOSR), U.S.A. (grant # FA2386-21-1-4070 to N.S.S. and C.F.C.), and the joint Orchid Project by NSTC and Bureau Français de Taipei, Taiwan (to T.L. and C.F.C.). We thank Ms. Jessica Nock Paniagua for helpful suggestions and proofreading the manuscript, and the technical support from the AS Advanced Nano/Micro-Fabrication and Characterization Lab.

## Appendix A. Supporting information

Supplementary data associated with this article can be found in the online version at doi:10.1016/j.snb.2023.134303.

## References

[1] D.S. Wang, S.K. Fan, Microfluidic surface plasmon resonance sensors: from principles to point-of-care applications, Sensors 16 (2016) 1175.
[2] E. Priyadarshini, N. Pradhan, Gold nanoparticles as efficient sensors in colorimetric detection of toxic metal ions: a review, Sens. Actuators B Chem. 238 (2017) 888–902.
[3] J. Kudr, O. Zitka, M. Klimanek, R. Vrba, V. Adam, Microfluidic electrochemical devices for pollution analysis-a review, Sens. Actuators B Chem. 246 (2017) 578–590.
[4] R.E. Fernandez, B.J. Sanghavi, V. Farmehini, J.L. Chávez, J.A. Hagen, N. Kelley-Loughnane, et al., Aptamer-functionalized graphene-gold nanocomposites for label-free detection of dielectrophoretic-enriched neuropeptide Y, Electrochem. Commun. 72 (2016) 144–147.
[5] M. Jarczewska, Ł. Górski, E. Malinowska, Electrochemical aptamer-based biosensors as potential tools for clinical diagnostics, Anal. Methods 8 (2016) 3861–3877.
[6] K.M. Koo, A.A.I. Sina, L.G. Carrascosa, M.J.A. Shiddiky, M. Trau, DNA–bare gold affinity interactions: mechanism and applications in biosensing, Anal. Methods 7 (2015) 7042–7054.
[7] Y. Zhang, H. Hong, W. Cai, Tumor-targeted drug delivery with aptamers, Curr. Med. Chem. 18 (2011) 4185–4194.
[8] A. Latorre, C. Posch, Y. Garcimartin, A. Celli, M. Sanlorenzo, I. Vujic, et al., DNA and aptamer stabilized gold nanoparticles for targeted delivery of anticancer therapeutics, Nanoscale 6 (2014) 7436–7442.
[9] N. Elahi, M. Kamali, M.H. Baghersad, Recent biomedical applications of gold nanoparticles: a review, Talanta 184 (2018) 537–556.
[10] Y. Xue, X. Li, H. Li, W. Zhang, Quantifying thiol-gold interactions towards the efficient strength control, Nat. Commun. 5 (2014) 4348.
[11] N.S. Swami, C.F. Chou, R. Terbrueggen, Two-potential electrochemical probe for study of DNA immobilization, Langmuir 21 (2005) 1937–1941.
[12] C.D. Bain, E.B. Troughton, Y.T. Tao, J. Evall, G.M. Whitesides, R.G. Nuzzo, Formation of monolayer films by the spontaneous assembly of organic thiols from solution onto gold, J. Am. Chem. Soc. 111 (1989) 321–335.
[13] C.D. Bain, G.M. Whitesides, Molecular-level control over surface order in self-assembled monolayer films of thiols on gold, Science 240 (1988) 62–63.
[14] A.W. Peterson, R.J. Heaton, R.M. Georgiadis, The effect of surface probe density on DNA hybridization, Nucleic Acids Res. 29 (2001) 5163–5168.
[15] Z.F. Gao, J.B. Gao, L.Y. Zhou, Y. Zhang, J.C. Si, H.Q. Luo, et al., Rapid assembly of ssDNA on gold electrode surfaces at low pH and high salt concentration conditions, RSC Adv. 3 (2013) 12334–12340.
[16] S.J. Hurst, A.K.R. Lytton-Jean, C.A. Mirkin, Maximizing DNA loading on a range of gold nanoparticle sizes, Anal. Chem. 78 (2006) 8313–8318.
[17] X. Zhang, M.R. Servos, J. Liu, Instantaneous and quantitative functionalization of gold nanoparticles with thiolated DNA using a pH-assisted and surfactant-free route, J. Am. Chem. Soc. 134 (2012) 7266–7269.
[18] G. Luka, A. Ahmadi, H. Najjaran, E. Alocilja, M. DeRosa, K. Wolthers, et al., Microfluidics integrated biosensors: a leading technology towards lab-on-a-chip and sensing applications, Sensors 15 (2015) 30011–30031.
[19] N.T. Darwish, S.D. Sekaran, S.M. Khor, Point-of-care tests: a review of advances in the emerging diagnostic tools for dengue virus infection, Sens. Actuators B

Chem. 255 (2018) 3316–3331.
[20] E.K. Sackmann, A.L. Fulton, D.J. Beebe, The present and future role of microfluidics in biomedical research, Nature 507 (2014) 181–189.
[21] K. Mawatari, Y. Kazoe, H. Shimizu, Y. Pihosh, T. Kitamori, Extended-nanofluidics: fundamental technologies, unique liquid properties, and application in chemical and bio analysis methods and devices, Anal. Chem. 86 (2014) 4068–4077.
[22] X.Y. Chen, L. Zhang, Review in manufacturing methods of nanochannels of bio-nanofluidic chips, Sens. Actuators B Chem. 254 (2018) 648–659.
[23] L.J. Guo, X. Cheng, C.F. Chou, Fabrication of size-controllable nanofluidic channels by nanoimprinting and its application for DNA stretching, Nano Lett. 4 (2004) 69–73.
[24] H. Daiguji, Ion transport in nanofluidic channels, Chem. Soc. Rev. 39 (2010) 901–911.
[25] R. Peng, D. Li, Electroosmotic flow in single PDMS nanochannels, Nanoscale 8 (2016) 12237–12246.
[26] L.J. Cheng, L.J. Guo, Rectified ion transport through concentration gradient in homogeneous silica nanochannels, Nano Lett. 7 (2007) 3165–3171.
[27] W. Sparreboom, A. van den Berg, J.C.T. Eijkel, Principles and applications of nanofluidic transport, Nat. Nanotechnol. 4 (2009) 713–720.
[28] D. Stein, Z. Deurvorst, F.H. van der Heyden, W.J. Koopmans, A. Gabel, C. Dekker, Electrokinetic concentration of DNA polymers in nanofluidic channels, Nano Lett. 10 (2010) 765–772.
[29] K.T. Liao, C.F. Chou, Nanoscale molecular traps and dams for ultrafast protein enrichment in high-conductivity buffers, J. Am. Chem. Soc. 134 (2012) 8742–8745.
[30] W. Reisner, K.J. Morton, R. Riehn, Y.M. Wang, Z.N. Yu, M. Rosen, et al., Statics and dynamics of single DNA molecules confined in nanochannels, Phys. Rev. Lett. 94 (2005) 196101.
[31] F. Persson, J. Fritzsche, K.U. Mir, M. Modesti, F. Westerlund, J.O. Tegenfeldt, Lipid-based passivation in nanofluidics, Nano Lett. 12 (2012) 2260–2265.
[32] R.B. Schoch, L.F. Cheow, J. Han, Electrical detection of fast reaction kinetics in nanochannels with an induced flow, Nano Lett. 7 (2007) 3895–3900.
[33] T. Leichle, C.F. Chou, Biofunctionalized nanoslits for wash-free and spatially resolved real-time sensing with full target capture, Biomicrofluidics 9 (2015) 034103.
[34] R. Peng, D. Li, Detection and sizing of nanoparticles and DNA on PDMS nanofluidic chips based on differential resistive pulse sensing, Nanoscale 9 (2017) 5964–5974.
[35] R. Oz, S. Kk, F. Westerlund, A nanofluidic device for real-time visualization of DNA-protein interactions on the single DNA molecule level, Nanoscale 11 (2019) 2071–2078.
[36] J.O. Tegenfeldt, C. Prinz, H. Cao, S. Chou, W.W. Reisner, R. Riehn, et al., The dynamics of genomic-length DNA molecules in 100-nm channels, Proc. Natl. Acad. Sci. U.S.A. 101(2004) 10979–10983.
[37] T. Yasui, N. Kaji, Y. Baba, Nanobiodevices for biomolecule analysis and imaging, Annu. Rev. Anal. Chem. 6 (2013) 83–96.
[38] J. Han, H.G. Craighead, Separation of long DNA molecules in a microfabricated entropic trap array, Science 288 (2000) 1026–1029.
[39] B.J. Sanghavi, W. Varhue, A. Rohani, K.T. Liao, L.A. Bazydlo, C.F. Chou, et al., Ultrafast immunoassays by coupling dielectrophoretic biomarker enrichment in nanoslit channel with electrochemical detection on graphene, Lab Chip 15 (2015) 4563–4570.
[40] A. Rohani, B.J. Sanghavi, A. Salahi, K.T. Liao, C.F. Chou, N.S. Swami, Frequency-selective electrokinetic enrichment of biomolecules in physiological media based on electrical double-layer polarization, Nanoscale 9 (2017) 12124–12131.
[41] Y.L. Lin, Y.J. Huang, P. Teerapanich, T. Leichle, C.F. Chou, Multiplexed immunosensing and kinetics monitoring in nanofluidic devices with highly enhanced target capture efficiency, Biomicrofluidics 10 (2016) 034114.
[42] P. Teerapanich, M. Pugniere, C. Henriquet, Y.L. Lin, C.F. Chou, T. Leichle, Nanofluidic fluorescence microscopy (NFM) for real-time monitoring of protein binding kinetics and affinity studies, Biosens. Bioelectron. 88 (2017) 25–33.
[43] J. Cacheux, M. Brut, A. Bancaud, P. Cordelier, T. Leichle, Spatial analysis of nanofluidic-embedded biosensors for wash-free single-nucleotide difference discrimination, ACS Sens 3 (2018) 606–611.
[44] H. Du, M.D. Disney, B.L. Miller, T.D. Krauss, Hybridization-based unquenching of DNA hairpins on Au surfaces: prototypical "molecular beacon" biosensors, J. Am. Chem. Soc. 125 (2003) 4012–4013.
[45] B. Dubertret, M. Calame, A.J. Libchaber, Single-mismatch detection using gold-quenched fluorescent oligonucleotides, Nat. Biotechnol. 19 (2001) 365–370.
[46] E. Dulkeith, A.C. Morteani, T. Niedereichholz, T.A. Klar, J. Feldmann, S.A. Levi, et al., Fluorescence quenching of dye molecules near gold nanoparticles: Radiative and nonradiative effects, Phys. Rev. Lett. 89 (2002) 203002.
[47] L. Huang, D.B. Wang, N. Singh, F. Yang, N. Gu, X.E. Zhang, A dual-signal amplification platform for sensitive fluorescence biosensing of leukemia-derived exosomes, Nanoscale 10 (2018) 20289–20295.
[48] D.K. Yang, C.F. Chou, L.C. Chen, Selection of aptamers for AMACR detection from DNA libraries with different primers, RSC Adv. 8 (2018) 19067–19074.
[49] T. Leichle, Y.L. Lin, P.C. Chiang, S.M. Hu, K.T. Liao, C.F. Chou, Biosensor-compatible encapsulation for pre-functionalized nanofluidic channels using asymmetric plasma treatment, Sens. Actuators B Chem. 161 (2012) 805–810.
[50] J. Gu, R. Gupta, C.F. Chou, Q.H. Wei, F. Zenhausern, A simple polysilsesquioxane sealing of nanofluidic channels below 10 nm at room temperature, Lab Chip 7 (2007) 1198–1201.
[51] R. Marie, H. Jensenius, J. Thaysen, C.B. Christensen, A. Boisen, Adsorption kinetics and mechanical properties of thiol-modified DNA-oligos on gold investigated by microcantilever sensors, Ultramicroscopy 91 (2002) 29–36.
[52] D.Y. Petrovykh, H. Kimura-Suda, L.J. Whitman, M.J. Tarlov, Quantitative analysis and characterization of DNA immobilized on gold, J. Am. Chem. Soc. 125 (2003) 5219–5226.
[53] G.L. Lukacs, P. Haggie, O. Seksek, D. Lechardeur, N. Freedman, A.S. Verkman, Size-dependent DNA mobility in cytoplasm and nucleus, J. Biol. Chem. 275 (2000) 1625–1629.
[54] S. Sjolander, C. Urbaniczky, Integrated fluid handling-system for biomolecular interaction analysis, Anal. Chem. 63 (1991) 2338–2345.
[55] Y. Zhang, H.J. Zhou, Z.C. Ou-Yang, Stretching single-stranded DNA: interplay of electrostatic, base-pairing, and base-pair stacking interactions, Biophys. J. 81 (2001) 1133–1143.
[56] O. Isaienko, E. Borguet, Hydrophobicity of hydroxylated amorphous fused silica surfaces, Langmuir 29 (2013) 7885–7895.
[57] B. Shi, Y.K. Shin, A.A. Hassanali, S.J. Singer, DNA binding to the silica surface, J. Phys. Chem. B 119 (2015) 11030–11040.
[58] A.B. Steel, T.M. Herne, M.J. Tarlov, Electrochemical quantitation of DNA immobilized on gold, Anal. Chem. 70 (1998) 4670–4677.
[59] M. Chen, Y.Y. Wang, H.L. Su, L. Mao, X.N. Jiang, T. Zhang, et al., Three-dimensional electrochemical DNA biosensor based on 3D graphene-Ag nanoparticles for sensitive detection of CYFRA21-1 in non-small cell lung cancer, Sens. Actuators B Chem. 255 (2018) 2910–2918.
[60] L.C. Bock, L.C. Griffin, J.A. Latham, E.H. Vermaas, J.J. Toole, Selection of single-stranded-DNA molecules that bind and inhibit human thrombin, Nature 355 (1992) 564–566.

**Deng-Kai Yang** is a Postdoctoral Fellow at the Institute of Physics, Academia Sinica, Taiwan. He is dedicated to research on micro/nanofluidics, surface chemistry, and molecular technology for application in biosensing and aptamer discovery. https://orcid.org/0000–0001–5161–8052.

**Liang-Kun Yu** is a Ph.D. student of the Taiwan International Graduate Program (TIGP)-Nano S&T Program at the Institute of Physics, Academia Sinica, Taiwan. He focuses on nano-fabrication to develop a single-molecule detector and is familiar with design micro/nanofluidics devices for bio-sensor.

**Chia-Tzu Kuo** is a Research Assistant at the Institute of Physics, Academia Sinica, Taiwan. He focuses on nano-fabrication and is familiar with design micro/nanofluidics devices for bio-sensor.

**Jui-Hong Weng** is a Postdoctoral Fellow at the Institute of Physics, Academia Sinica, Taiwan. He focuses on biosensing research and is familiar with protein modification, nano-fabrication, electrochemical sensing and aptamer selection.

**Thierry Leïchlé** is a Research Fellow at LAAS-CNRS, France. His group works on MEMS biosensors to develop micro/nanoelectromechanical systems, and fluidic devices for biotechnology applications, *e.g.*, biomolecular patterning, sensing, and imaging. https://scholar.google.com.tw/citations?hl=en&user=yjtUa34AAAAJ

**Nathan S. Swami** is a Professor of Electrical & Computer Engineering at the University of Virginia, Charlottesville, VA. His group seeks to develop electrically functional microfluidic devices and instrumentation for label-free manipulation, sorting, and cytometry of biosystems, for applications in biomolecular sensing, *in vitro* disease modeling, and integrative tissue regeneration. https://scholar.google.co.in/citations?user=iS12HRMAAAAJ&hl=en

**Lin-Chi Chen** is a Professor at the Department of Biomechatronics Engineering, National Taiwan University, Taiwan. His group is dedicated to technology development for intelligent biosensing, ion-sensing, and other interdisciplinary studies. https://scholar.google.com.tw/citations?hl=en&user=sg8sq20AAAAJ

**Pei-Kuen Wei** is a Research Fellow/Professor and Director at the Research Center of Applied Sciences, Academia Sinica, Taiwan. His group seeks to develop nearfield optics, nano-photonics, and related techniques to apply to nanostructures biosensing, bioimaging, and green-energy researches. https://scholar.google.com.tw/citations?hl=en&user=oPf5dn8AAAAJ.

**Chia-Fu Chou** is a Distinguished Research Fellow/Professor at the Institute of Physics, Academia Sinica, Taiwan. His research group specializes in biophysics, biophotonics, nanobiotechnology, micro/nanofluidics, liquid crystals researches. https://scholar.google.co.in/citations?user=kNMlPDAAAAAJ&hl=en.